Ore Geology Reviews 184 (2025) 106728

Contents lists available at ScienceDirect

Ore Geology Reviews

journal homepage: www.elsevier.com/locate/oregeorev

# Wall-rock control on the mineral assemblage of hydrothermal veins: examples from the Mahuaping Be-W-F deposit, Yunnan, SW China

Sheng Li [a,b], Rolf L. Romer [c], Wenchang Li [a,b,*], Fucheng Yang [a], Qinggao Yan [a], Huawen Cao [a,d], Shenjin Guan [a]

[a] School of Land and Resources Engineering, Kunming University of Science and Technology, Kunming 650093, China
[b] Department of Natural Resources and Environment, Southwest United Graduate School, Kunming 650092, China
[c] GFZ German Research Centre for Geosciences, 14473 Potsdam, Germany
[d] College of Earth Sciences, Chengdu University of Technology, Chengdu 610059, China

ARTICLE INFO

*Keywords:*
Beryllium-tungsten-fluorine deposit
Mica
Scheelite
Ore-forming fluid
Vein-type mineralization

ABSTRACT

The 32 Ma vein-type Mahuaping Be-W-F deposit is closely related to the folding and faulting of its host-rocks, Ordovician slates and Silurian limestones. We demonstrate that mineral assemblages in the veins are controlled by the wall-rocks and argue that fluid-rock interaction triggered mineral precipitation. Veins show two stages of mineralization. Stage I mica-quartz veins with beryl, scheelite and fluorite occur in limestone, slate, and their contact zone. Dissolution of limestone provided Ca to form scheelite and fluorite in veins in the limestones and in the contact zone. The precipitation of fluorite destabilized Be-fluoride complexes in the fluid and induced the precipitation of beryl. Alteration of slates provided Fe to produce wolframite in veins hosted in slates and in the contact zone. The composition of Stage I mica ranges from muscovite in veins in the limestones to phengite in veins in the slates. The trace element contents of Stage I mica depend on the nature of the wall rocks. Stage II mica-quartz veins are barren. Stage II veins are shielded from interaction with the wall-rocks by Stage I mineral assemblages. Therefore, the composition of Stage II muscovite and its trace-element signature are independent of the nature of the wall-rocks. The trace element inventory of Stage II mica indicates that the mineralizing fluid, which carried the ore elements Be, W, F, and Sn, is derived from low-grade sedimentary rocks rather than an unexposed intrusion.

## 1. Introduction

The compositions of muscovite and scheelite are widely used to trace the source and the chemical properties of ore-forming fluids (Gomes and Neiva, 2000; Dostal et al., 2009; Li et al., 2021a; Dai et al., 2022; Peng et al., 2023; Ji et al., 2024). The trace element signatures of muscovite and scheelite provide complementary information, as the scavenging of fluid soluble elements depends on the compatibility of these elements in the crystal structure. For instance, elements that readily substitute for Ca may be strongly underrepresented in muscovite and strongly enriched in scheelite. Because the interaction of fluids with the wall-rocks changes the composition of the fluid, the composition of muscovite may carry a mixed signature reflecting the fluid source, the local wall-rocks, and possible element scavenging by earlier precipitated minerals. These reaction-induced changes of the fluid composition may result in the wall-rock control of the mineral assemblage of vein-type mineralization (Pirajno, 2009; Li et al., 2022).

We illustrate the influence of the wall-rocks on the mineral assemblage and mineral compositions of vein-type mineralization using the Mahuaping low-temperature Be-W-F deposit that is hosted in limestones and slates. This deposit is particularly suited to illustrate the wall-rock influence because of the following reasons: (i) The ore forming fluid flows in the contact zone between Ordovician slates and Silurian limestones and forms quartz-muscovite vein type mineralization in these rocks and irregular mineralization in the contact zone. As vein-type mineralization in both types of wall rocks is caused by the same fluid, differences in mineral assemblage and mineral composition are related to the nature of the wall rocks. (ii) The ore elements Be, W, and F have low contents in the wall rocks. Contributions from the wall rocks have little or no effect on the budget of these elements in the fluid. Thus, the availability of ore elements is controlled by the fluid, whereas the precipitation of the ore elements is controlled by the wall rocks. (iii) There

* Corresponding author at: School of Land and Resources Engineering, Kunming University of Science and Technology, Kunming 650093, China.
*E-mail address:* lwcyndd@163.com (W. Li).

https://doi.org/10.1016/j.oregeorev.2025.106728
Received 17 March 2025; Received in revised form 11 May 2025; Accepted 11 June 2025
Available online 16 June 2025

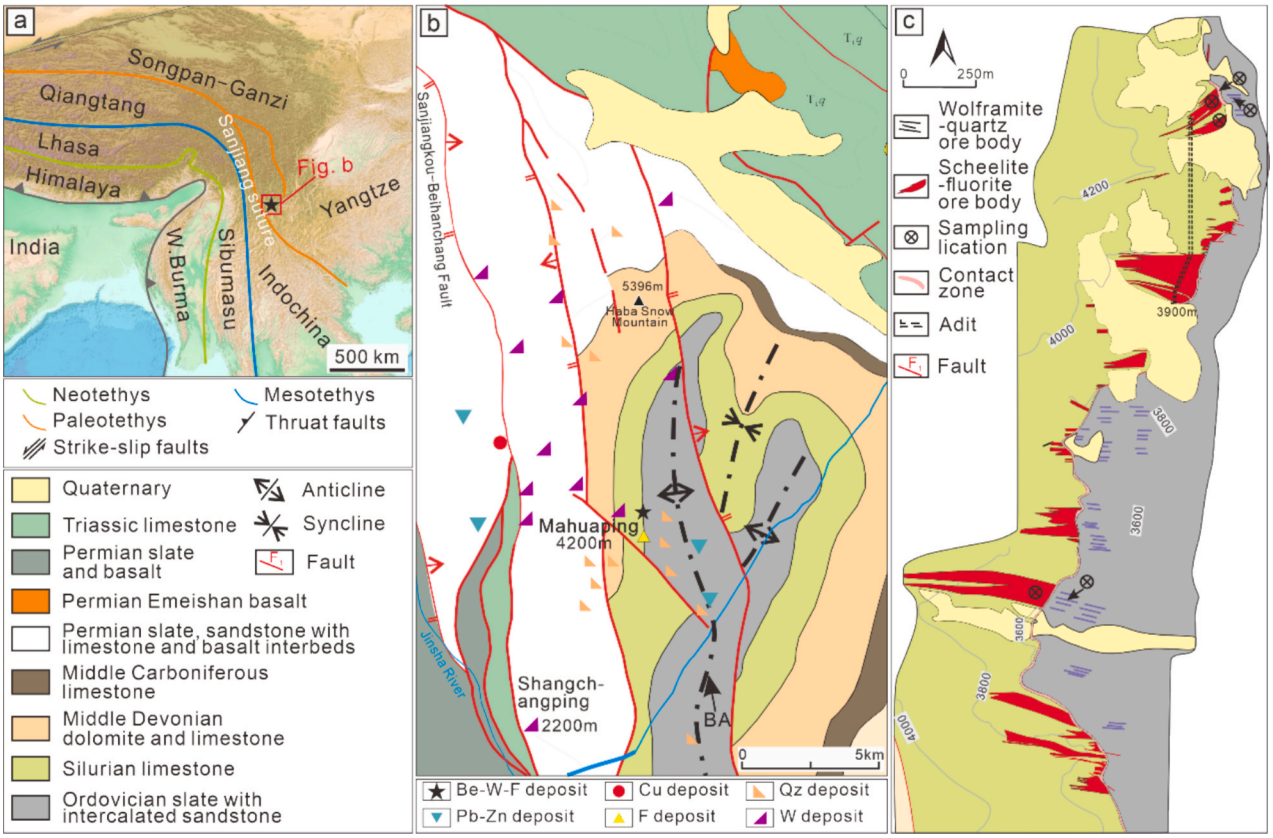


**Fig. 1.** (a) Simplified tectonic map showing the position of major Tethys sutures and the location the Sanjiang belt and the Mahuaping deposit (Yang et al., 2025). (b) Simplified geological map of the Mahuaping area. BA = Bendiwan anticline. (c) Geological map of the Mahuaping deposit showing the distribution of ore bodies (modified after Bureau of Geology and Mineral Resources of Yunnan Province, 2017).

are two generations of vein-type mineralization in limestones and slates. Fluids forming the first generation of mica interacted with the wall rocks; fluids forming the second generation of mica were shielded from wall-rock interaction by first-generation mineralization.

We describe the mineralogical characteristics of the veins and present EPMA and LA-ICP-MS in situ major and trace element data of muscovite from the veins in the limestones and slates and their contact zone, as well as EPMA and LA-ICP-MS in situ major and trace element data of scheelite from the veins in the limestones and the contact zone. Our data show that the mineral assemblages of the veins are directly influenced by the dissolution or alteration the immediate wall rocks. This interaction is obvious from the occurrence of scheelite in veins in the limestones and wolframite in veins in the slates, but also in the chemical composition of different generations of mica in veins hosted by different lithologies. We use the trace element composition of mica from both generations of vein-type mineralization to argue that the ore elements Be, W, Sn, and F were mobilized during regional deformation and metamorphism and do not originate from an unexposed intrusion.

## 2. Geological background

### 2.1. Setting of the Mahuaping Be-W-F deposit

The Sanjiang ("Three River") region in the western part of the Yunnan Province (Fig. 1) contains a collage of Paleozoic terranes and Gondwana-derived blocks that were accreted to the Yangtze bock along the Paleo-Tethys (c. 250 Ma), Meso-Tethys (c. 130–120 Ma), and Neo-Tethys (c. 80 Ma) sutures (Li et al., 2016; Li et al., 2021a). The complex tectonic development in the Sanjiang belt, involves not only the accretion and collision of terranes and continental blocks, but also the reactivation of older sutures and the deformation of the accreted units and the margin of the Yangtze craton during the closure of younger Tethys branches, the collision of India, and the uplift of Tibet (Metcalfe, 2013). The last major reactivation occurred at about 30 Ma (Metcalfe, 2013; Li et al., 2016).

The Mahuaping Be-W-F deposit is located near the axis of the Benziwan anticline (BA in Fig. 1). The c. 32 Ma deposit is hosted in Ordovician slates and Silurian limestones that have undergone low-grade metamorphism (Ma et al., 2020). During folding, rocks of the contact zone between the slates and limestones, i.e., calcareous and siliceous mudstones, developed into a large-scale detachment fault that provided pathways for fluids released from deeper prograde metamorphosed units (Figs. 1 and 2). Folding and interlayer shearing resulted in the formation of tensional fractures in the slates and in particular in the brittle carbonates. These fractures are at a high angle to the shear zone and to the bedding of the sedimentary rocks (Fig. 2). The Be-W-F mineralization is structurally controlled. It is bound to the contact zone between shale and limestone and the fissures in the wall rocks. The limestones, which form the local hanging-wall rocks, had recrystallized in the contact zone and were bleached near the contact zone (Fig. 2) (Xiong et al., 2015; Ma et al., 2020; Jia et al., 2020). Intermediate to acid magmatic rocks are not exposed in the mining area and its surroundings.

### 2.2. Deposit geology

The Mahuaping Be-W-F deposit exhibits large-scale mineralization in the western limb of the Benziwan anticline. The deposit is exposed at elevations up to 4200 m and is known to extend at least down to 2200 m above sea level. In the mining area, mineralization of Be, W, and F coexists. The proven reserves are 41,700 tons of Be (containing 0.24 % BeO), 72,700 tons of W (containing 0.82 % $WO_3$), and 2,368,100 tons of $CaF_2$ (containing 16.95 % $CaF_2$) (Bureau of Geology and Mineral

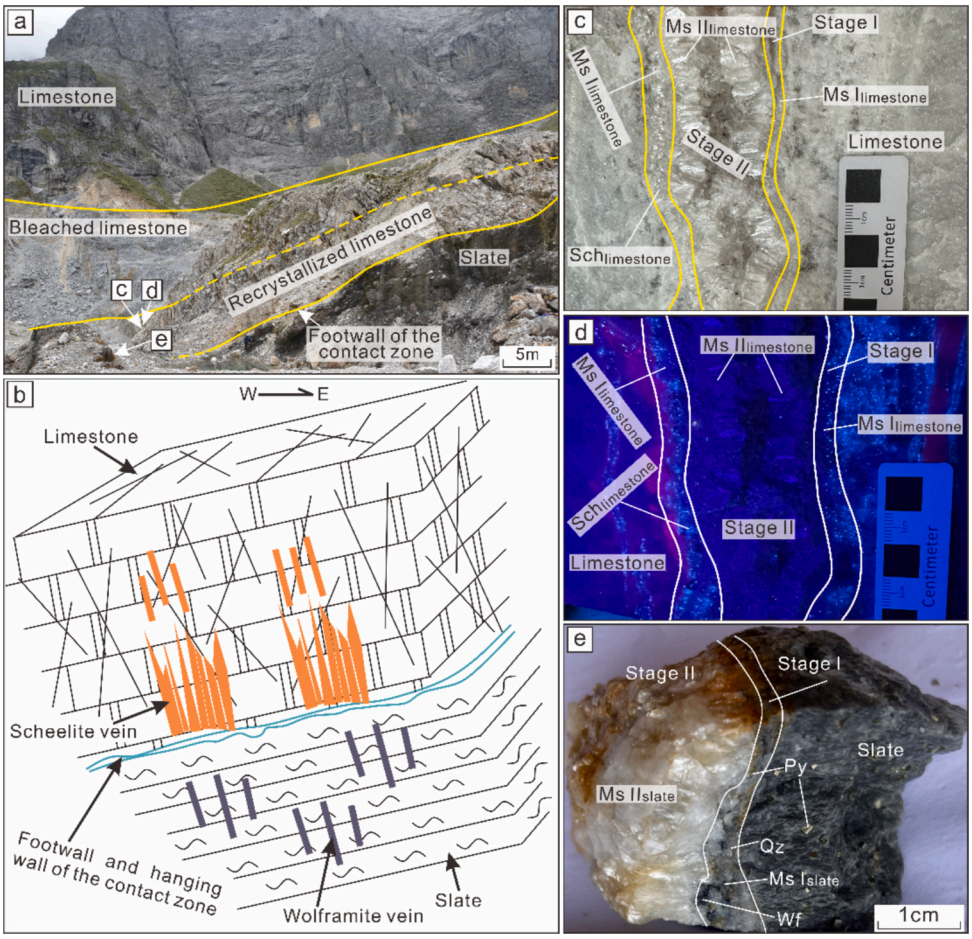


**Fig. 2.** (a) Field photograph of the Mahuaping Be-W-F deposit illustrating the relation between slates, contact zone, and limestones. Note the bleaching of the limestone is due to the loss of exsolved $H_2O$-$CO_2$ fluid from the contact zone and the veins. (b) Schematic block diagram illustrating the relation between bedding, tensional fissures, and mineralization. The contrasting distribution of mineralization in the footwall and hanging-wall is caused by the contrasting rheology of slates and limestones. (c-d) Two-stage vein in limestone (natural and UV light, respectively). Stage II mica is coarse-grained; scheelite (tiny bright-blue spots in UV light) occurs only in Stage I mineralization. (e) Two-stage vein in slate. (For interpretation of the references to colour in this figure legend, the reader is referred to the web version of this article.)

Resources of Yunnan Province, 2017). The stratigraphic sequence that is exposed includes siliciclastic rocks, carbonate rocks, and basalts, all of which have undergone low-grade metamorphism. The lowest exposed units are Ordovician slates and schists. These are overlain by Silurian limestones and dolomites, which are further covered by Devonian sedimentary rocks to the east. Mineralization primarily occurs within the Ordovician slates, Silurian limestones, and the contact zone between them (Ran et al., 2011; Xiong et al., 2015; Jia et al., 2020; Ma et al., 2020). The Mahuaping deposit stretches for three kilometers along a north–south trending fault, has a width of up to one kilometer, and includes 33 individual ore bodies. These ore bodies are composed of sections with particularly densely spaced or wide veins. These ore bodies are concentrated along the contact zone and extend from the contact zone in a comb-like or wedge-shaped pattern into the limestones and slates of the western limb of the Bendiwan anticline (Figs. 1 and 2) (Ran et al., 2011; Ma et al., 2020).

The deposit includes three types of mineralization, i.e., (i) 0.1 to 1 cm wide scheelite-fluorite-muscovite-quartz veins in the limestones, (ii) up to 10 cm wide wolframite-muscovite-quartz veins in the slates, and (iii) beryl (euclase)-scheelite-wolframite-fluorite-quartz mineralization in the contact zone between limestones and slates. Mineralization within the limestones consists of numerous, closely spaced scheelite-fluorite-muscovite-quartz veins that are nearly perpendicular to the original bedding of the carbonate rocks. In contrast, mineralization in the slates is characterized by relatively sparse muscovite-wolframite-quartz veins. In these veins, beryl occurs only near the contact zone. The veins exhibit distinct zoning with a marginal zone of fine-grained muscovite and quartz and a core of coarse-grained muscovite and quartz (Fig. 2d-e). In contrast, in the contact zone there is no zonation and the mineralization is dominated by fine-grained muscovite and quartz. Only zones with fine-grained muscovite also have ore minerals. Although vein-type mineralization in the limestones and the slates, as well as mineralization in the contact zone, were generated by the fluids that migrated along the detachment fault, the three types of mineralization have contrasting assemblages or ore minerals. Veins in limestone carry the ore minerals scheelite, beryl, and fluorite, whereas veins in slate mainly carry wolframite. In the contact zone, there is scheelite and wolframite.

## 3. Samples and analytical methods

We collected mineralized quartz-muscovite veins in the Mahuaping mining area at the 4200 m surface and the 3600 m underground levels. In addition, we sampled mineralization from the contact zone between the limestone and the slates (Fig. 3). Based on field and microscopic observations, the mineral assemblage in the veins formed during two hydrothermal stages, an early ore-bearing stage with fine-grained muscovite and a late barren stage with coarse-grained muscovite (Table 1; Fig. 4). Hydrothermal mineral precipitates in the contact zone belong to the early stage and contain only fine-grained muscovite. Scheelite occurs in limestone-hosted veins and the contact zone. We

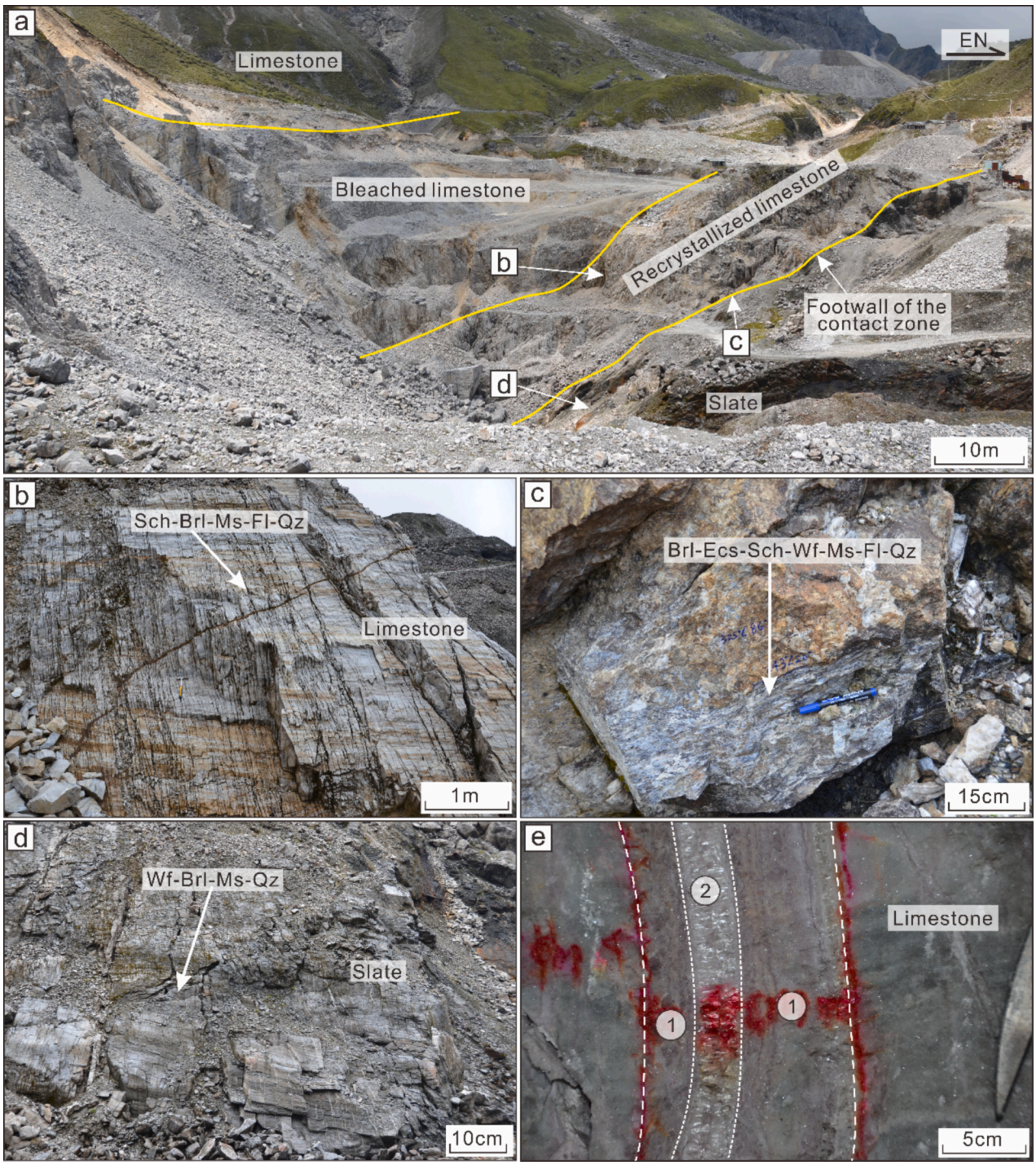


**Fig. 3.** Field characteristics of the Mahuaping deposit. (a) Contact relations at the 4200 m level. (b) Sch-Brl-Ms-Fl-Qz veins (dark) nearly perpendicular to the bedding of their limestone host-rocks. (c) Brl-Eu-Sch-Wf-Ms-Fl-Qz veins developed at the contact zone between limestone and slate. (d) Wf-Brl-Ms-Qz veins developed in siliciclastic rocks. (e) Fine-grained (1) and coarse-grained (2) muscovite veins hosted in limestone.

determined the chemical composition of muscovite from both stages of the two vein types and from the contact zone. In addition, we analyzed scheelite from limestone-hosted veins and the contact zone.

### 3.1. Major element analysis of muscovite and scheelite

Mineral compositions were determined using a JEOL JXA-8230 Electron Probe Microanalyzer (EMPA) equipped with five wavelength-dispersive spectrometers (WDS) at the Laboratory of Microscopy and Microanalysis, Wuhan Microbeam Analysis Technology Co. Ltd., Wuhan, China. The samples were coated with a c. 20 nm thin carbon film prior to analysis. For EPMA analytical details see Yang et al. (2022). For quantitative analyses, the EPMA was operated at 15 kV acceleration voltage, 10 nA beam current, and 10 μm spot size. Data were corrected online using a ZAF (atomic number, absorption, fluorescence) correction procedure. The peak counting times were 10 s for Ca, K, Mg, Na, Si, Al, Fe, F, Cl, Rb, Cs, Cr, and P and 20 s for Ti and Mn. Backgrounds were measured at the high- and low-energy side of the peak for half of the peak counting time. The following standards were used: Rutile (Ti), diopside (Ca, Mg), microcline (K), jadeite (Na), almandine (Fe), olivine

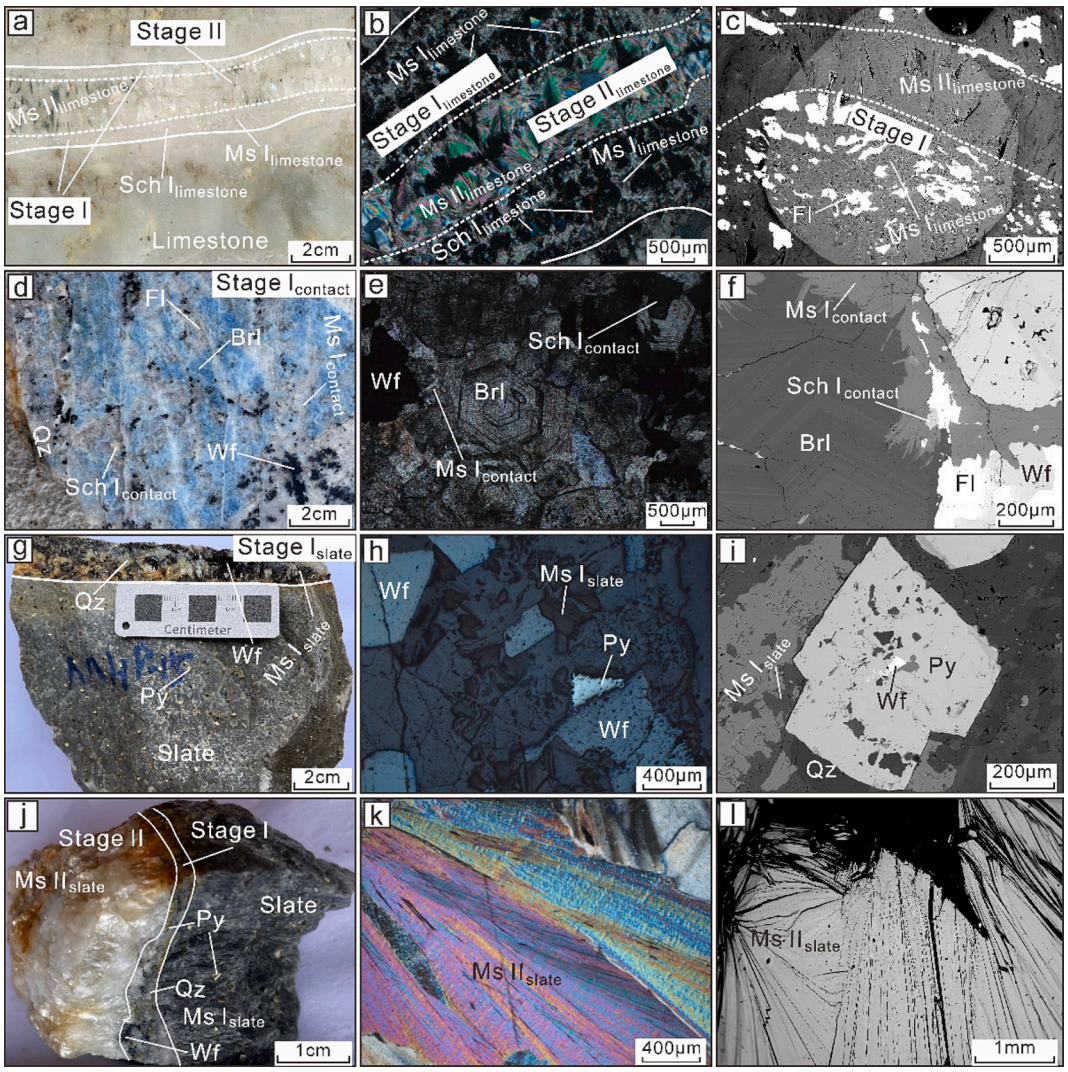


**Fig. 4.** Characterization of different vein stages in the Mahuaping deposit. (a) Hand specimen, (b) microphotograph, and (c) BSE image of Sch-Brl-Ms-Fl ± Qz vein with rich ore in early fine-grained muscovite (Stage $I_{limestone}$) and lean ore in late coarse-grained muscovite (Stage $II_{limestone}$). (d) Hand specimen, (e) microphotograph, and (f) BSE image of Brl-Sch-Wf-Ms-Fl ± Qz vein in the contact zone (Stage $I_{contact}$) between limestone and slate. (g) Handspecimen, (h) microphotograph, and (i) BSE image of Wf Brl-Ms-Qz-Cal vein (Stage $I_{slate}$) in siliciclastic host-rock. (j) Hand specimen, (k) microphotograph, and (l) BSE image of Wf-Py-Ms-Qz vein with rich ore in early fine-grained muscovite (Stage $I_{slate}$) and lean ore in late coarse-grained muscovite (Stage $II_{slate}$).

(Si), rhodonite (Mn), pyrope (Al), tugtupite (Cl), barium fluoride (F), pollucite (Cs), phosphate (Rb), chromium metal (Cr), and apatite (P).

### 3.2. LA-ICP-MS trace element analysis of muscovite and scheelite

Trace element analysis of muscovite and scheelite were conducted by LA-ICP-MS at the Wuhan Sample Solution Analytical Technology Co. Ltd., Wuhan, China. Detailed operating conditions for the laser ablation system, the ICP-MS instrument, and data reduction are described by Zong et al. (2017). Laser sampling was performed using a GeolasPro laser ablation system that consists of a COMPexPro 102 ArF excimer laser (193 nm wavelength and 200 mJ maximum energy) and a Micro-Las optical system. An Agilent 7900 ICP-MS instrument was used to measure ion-signal intensities. Helium was applied as a carrier gas. Argon was used as make-up gas and mixed with the carrier gas via a T-connector before entering the ICP. A "wire" signal smoothing device was included in the laser ablation system (Hu et al., 2015). The laser was set to 44 μm spot size and operated at 5 Hz. Trace element contents of minerals were calibrated against various reference materials (BHVO-2G, BCR-2G, and BIR-1G) without using an internal standard (Liu et al., 2008). Each analysis included approximately 20 – 30 s of background acquisition followed by 50 s of data acquisition. The Excel-based software ICPMSDataCal was used to perform off-line selection and integration of background and sample signals, drift correction, and quantitative calibration for trace element analysis (Liu et al., 2008).

## 4. Results

### 4.1. Major- and trace-element compositions of muscovite

Major and trace element contents of muscovite were determined using EPMA and LA-ICP-MS, respectively. The measured totals of analyzed oxides fall in the range from 93.53 wt% to 96.45 wt%, which is typical for muscovite. The chemical formula of muscovite was calculated for 22 oxygen a.p.f.u. using the structural formulas of Lin and Peng (1994) and Tischendorf et al. (1997). The results are shown in Tables S1 and S2.

#### 4.1.1. Muscovite from veins in limestone

Stage I and Stage II muscovite define two separate trends emerging from the muscovite end-member composition into the muscovite field (Fig. 5). Stage I muscovite has 45.07–50.31 wt% $SiO_2$, 27.60–37.40 wt%

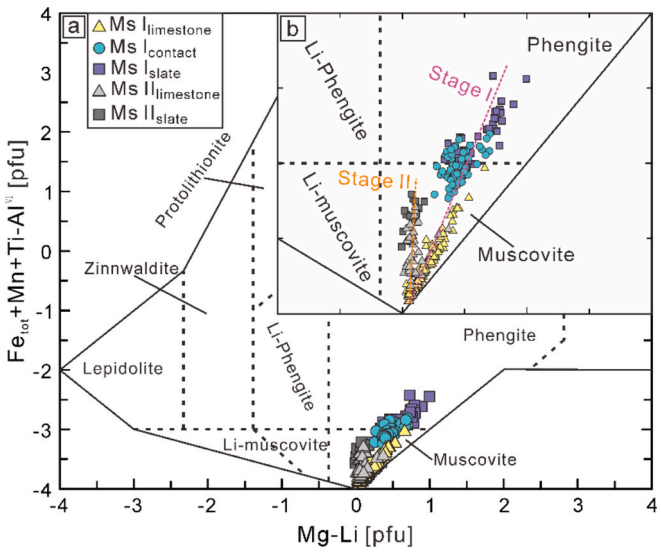


**Fig. 5.** (a) Full and (b) enlarged (Mg-Li) − ($Fe_{tot}$ + Mn + Ti + $Al^{VI}$) classification diagram showing the chemical composition of mica from veins in the Mahuaping deposit. The composition of early-stage mica changes systematically, depending on host rock (Stage $I_{limestone}$, Stage $I_{contact}$, and Stage $I_{slate}$), from muscovite to phengite. Late-stage mica (Stage $II_{limestone}$ and Stage $II_{slate}$) is muscovite.

$Al_2O_3$, and 10.6–11.7 wt% $K_2O$ and minor amounts of FeO (0.01–0.69 wt%), MgO (0.16–4.26 wt%), and MnO (<0.36 wt%) (Fig. 6). The F content is between 0.11 and 1.37 wt%. The trace elements contents vary among the various analyses by up to two orders of magnitude (Figs. 7, 8, and 9). The most important trace elements include W (14–103 μg/g), Li (7.17–748 μg/g), Be (34.6–87.6 μg/g), Rb (1276–1955 μg/g), Cs (39.5–103 μg/g), Nb (0.33–88.7 μg/g), Sn (3.52–471 μg/g), and Sr (2.95–38.5 μg/g). In particular, the contents on Be, Nb, W, Sn, and Sr are much higher than usually found in muscovite from granitic and metamorphic rocks (e.g., 3.63–22.9 μg/g Sn; 49.3–820 μg/g Li; typically less than 0.3 μg/g Sr; 6.27–138 μg/g Be; 9.48–57.3 μg/g Nb) (Yang et al., 2020; Xu et al., 2022; Monnier et al., 2022; Sun et al., 2023; Song et al., 2023; Ni et al., 2023).

The compositional range of Stage II muscovite broadly overlaps with the range of Stage I muscovite, but with $Al_2O_3$ (32.30–36.94 wt%) and FeO (0.48–2.33 wt%) reaching to higher contents and with $SiO_2$ (45.37–47.40 wt%) and MgO (0.15–2.41 wt%) having lower maximal contents. The F contents range from 0.20 to 0.88 wt%. The trace element contents of Stage II muscovite generally overlap with those of Stage I muscovite, but typically encompass narrower ranges that are lower for W (14.9–39.0 μg/g), Li (18.5–238 μg/g), Be (27.1–41.5 μg/g), Rb (1300–1683 μg/g), Cs (46.2–85.2 μg/g), and Sr (8.85–33.5 μg/g) and higher for Nb (43.7–124 μg/g) and Sn (259–687 μg/g).

#### 4.1.2. *Muscovite from veins in slates*

Stage I muscovite from veins in the slates falls on the same compositional trend as Stage I muscovite from veins in limestones, although at generally higher contents of $SiO_2$ (46.83–51.08 wt%), MgO (1.48–6.75 wt%), FeO (0.29–2.16 wt%), and F (0.86–2.54 wt%) and generally lower contents of $Al_2O_3$ (23.88–31.91 wt%) and $K_2O$ (9.71–11.70 wt%). The compositions correspond to phengite. Stage I muscovite from both lithologies show strong enrichment of the same trace elements. The contents of these trace elements partially overlap, although Stage I muscovite from veins in the slates have generally higher contents of Li (704–2253 μg/g), Be (46.1–172 μg/g), Rb (1700–2193 μg/g), and Cs (97.1–204 μg/g) and lower contents of W (11.5–47.4 μg/g), Sn (1.05–25.3 μg/g), Sr (0.86–21.5 μg/g), and Nb (0.10–4.13 μg/g) (Figs. 8 and 9).

Stage II muscovite from veins in the slates has broadly similar major element contents as Stage II muscovite from veins in the limestones, where Stage II muscovite independent of the host rock defines separate ranges (Fig. 6) and trends (Figs. 5, 7, and 8), respectively. The trace element contents of Stage II muscovite show–independent of host lithology–similar ranges of W (13.9–34.8 μg/g), Li (148.3–414 μg/g), Be (29.1–51.2 μg/g), Rb (1395–1883 μg/g), Cs (58.9–84.4 μg/g), Nb

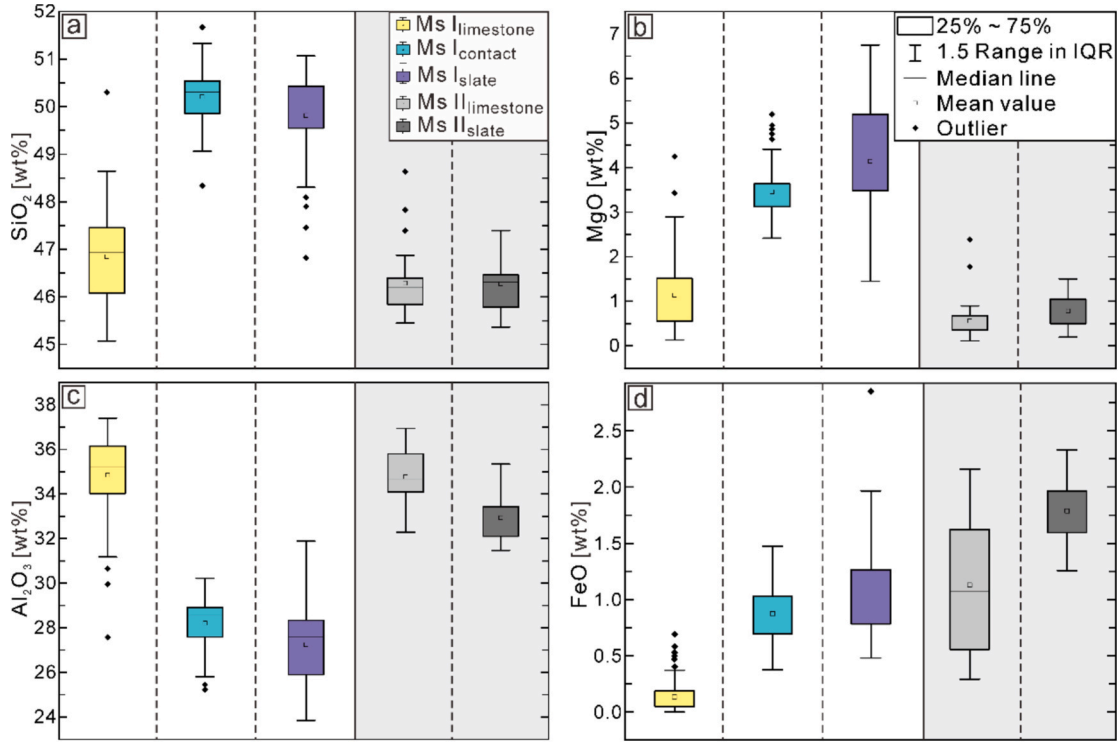


**Fig. 6.** Contents of $SiO_2$, MgO, $Al_2O_3$, and FeO in mica from the Mahuaping deposit.

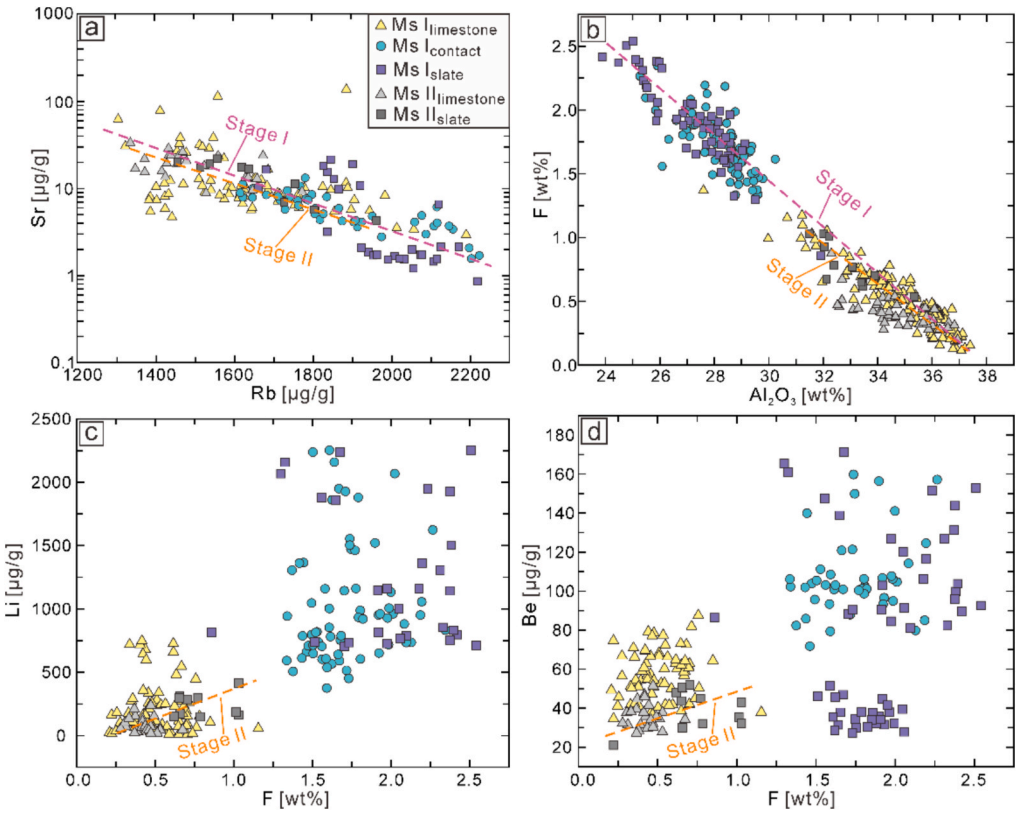


**Fig. 7.** Binary diagrams for mica from the Mahuaping deposit. (a) Rb vs. Sr, (b) $Al_2O_3$ vs. F, (c) F vs. Li, and (d) F vs. Be diagrams. Note the clustering of Stage II mica independent of the nature of the host rock and the difference between Stage I and Stage II mica from veins hosted by slates.

(2.43–106 μg/g), Sn (86.1–585 μg/g), and Sr (4.28–22.1 μg/g) (Figs. 8 and 9).

#### 4.1.3. Muscovite from the contact zone

In the contact zone, there is only Stage I muscovite whose composition in part overlaps with Stage I muscovite from veins in the slates and in part bridges the compositional gap to Stage I muscovite from veins in the limestones and the slates (Figs. 5, 6, 7, and 8). The ranges of major element compositions broadly overlap with those of Stage I muscovite from veins in the slates, although there is a tendency to lower $Al_2O_3$ (25.26–30.24 wt%) and higher MgO (2.44–5.21 wt%) and FeO (0.38–1.48 wt%) contents (Table S1). The trace element contents of muscovite in the contract zone are intermediate to those from the other two host-rocks as for Li (375–1624 μg/g) and Sr (1.57–13.2 μg/g) or similar to those of muscovite from veins in the slates, as for W (9.84–33.6 μg/g), Be (71.7–160 μg/g), Rb (1534–2180 μg/g), Cs (128–263 μg/g), Nb (0.04–1.76 μg/g), and Sn (0.66–17.5 μg/g) (Fig. 9).

### 4.2. Major- and trace-element compositions of scheelite

Scheelite may substitute Mo and high-field strength elements (HFSE), in particular Nb, Ta, U and REE, in variable and sometimes significant amounts for W and may substitute Sr and Pb for Ca. Other trace elements have low contents that are typically below 1 μg/g.

#### 4.2.1. Scheelite from veins in limestone

Scheelite only develops within veins and contact zones to the limestones and is restricted to Stage I veins in limestone. In addition to its primary components of $WO_3$ (78.11–80.65 wt%) and CaO (19.00–20.06 wt%), scheelite also contains trace amounts of $SiO_2$ (0.10–0.22 wt%) and F (below 0.76 wt%). It exhibits high Sr (213–1748 μg/g) and Pb (4.55–73.0 μg/g) contents, but low concentrations of Li (below 0.88 μg/g), Be (bdl–0.67 μg/g), Nb (1.04–21.3 μg/g), and Ta (0.02–0.11 μg/g; Table S3). The total rare earth element contents (ΣREE, La-Lu + Y) in scheelite range from 2.88 to 2200 μg/g. The light rare earth element contents (ΣLREE, La-Eu) are between 2.27 and 1888 μg/g, the middle rare earth element contents (ΣMREE, Gd-Ho) vary from 0.17 to 256 μg/g, and the heavy rare earth element concentrations (ΣHREE, Er-Yb) range from below detection limit to 56.8 μg/g (Fig. 10a).

#### 4.2.2. Scheelite from the contact zone

The contents of $MoO_3$, $SiO_2$, and F in scheelite from the contact zone (Sch $I_{contact}$) are all relatively low and similar to those of Sch $I_{limestone}$. In contrast, the Sr (1704–4694 μg/g) content of scheelite from the contact zone is significantly higher than of Sch $I_{limestone}$, and the trace element contents of Li (below 3.98 μg/g), Be (below 0.63 μg/g), Nb (6.32–9.75 μg/g), and Ta (0.02–0.11 μg/g) are all relatively low. Rare earth element contents (REEs), i.e., ΣREE, ΣLREE, ΣMREE, and ΣHREE, of Sch $I_{contact}$ are much higher than those of Sch $I_{limestone}$ (Table S3, Fig. 10).

## 5. Discussion

### 5.1. Wall-rock control on mineral assemblage of veins

At temperatures and pressures higher than at the Mahuaping deposit, interaction between fluids and carbonate wall-rocks leads to the formation of calc-silicate reaction rims and the release of large amounts of $CO_2$ and variable amounts of Ca and Sr into the fluids, leading to changes in the composition of the fluid and to phase separation for saline fluids (e.g., Heinrich 2007). In the Mahuaping area, however, temperature and pressure were too low to form calc-silicate reaction rims in the limestone. Instead, the carbonate wall-rocks dissolved during stage I. In the western section of the ore field (Fig. 2), $WO_4^{2-}$ and $F^-$ from the fluid combine with $Ca^{2+}$ derived from the limestone to produce substantial amounts of scheelite ($CaWO_4$) and fluorite ($CaF_2$). The high availability of Ca is the reason for the abundant precipitation of scheelite and

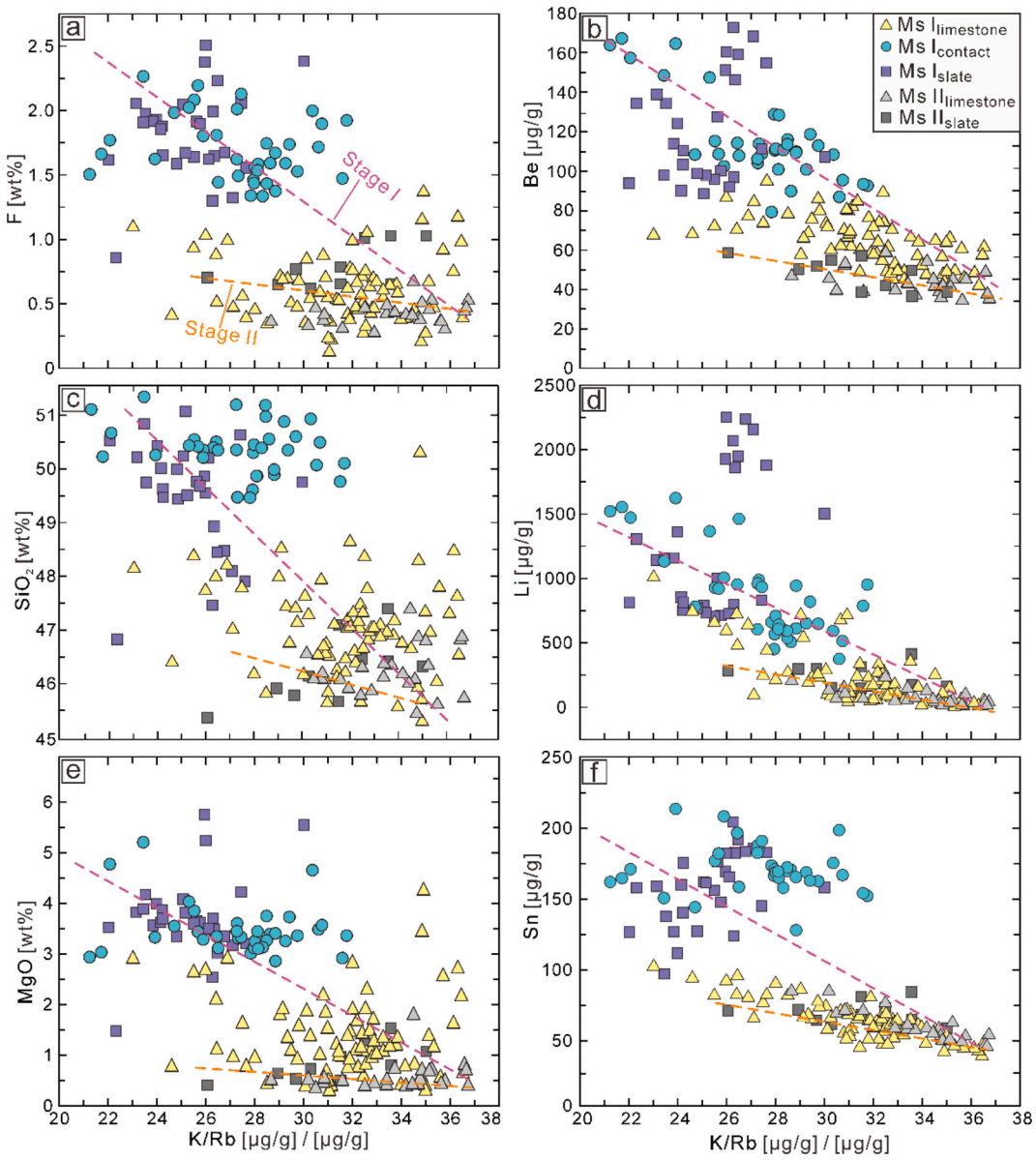


**Fig. 8.** Binary diagrams for mica from the Mahuaping deposit. (a) F vs. K/Rb, (b) Be vs. K/Rb, (c) $SiO_2$ vs. K/Rb, (d) Li vs. K/Rb, (e) MgO vs. K/Rb, and (f) Sn vs. K/Rb diagrams. Note the clustering of Stage II mica in dependence of the nature of the host rock and the difference between Stage I and Stage II mica from veins hosted by slates.

fluorite in the hydrothermal veins hosted by limestone. In contrast, in the eastern section of the ore field, the siliciclastic host rocks of the veins cannot provide Ca and $CO_2$. Instead, oxidation of sulfide minerals or alteration of mica in the clastic host-rocks supply significant amounts of Fe (and possibly Mn) to the fluid. In the veins in the siliciclastic host rocks, Fe and Mn combine with $WO_4^{2-}$ to form wolframite ((Fe,Mn)$WO_4$). In the contact zone, the fluids contain Ca and $CO_2$ from the limestone, as well as Fe and Mn from the clastic rocks. Therefore, mineralization in the contact zone includes scheelite, wolframite, beryl, and fluorite.

In low-temperature hydrothermal fluids, Be is most likely transported as fluoride ($BeF^+$, $BeF_2$, $BeF^{3-}$, and $BeF_4^{2-}$) or fluorocarbonate ($BeCO_3F^-$) complexes (Wood 1992). Fluorine-rich minerals such as fluorite, apatite, and muscovite in the hydrothermal veins of the Mahuaping deposit, indicate that F was present in the ore-forming fluids, facilitating the transport of W and Be from the source rocks to the vein-type mineralization (He et al., 2020). The precipitation of fluorite reduced the fluorine contents of the fluid, which destabilized fluoride and fluorocarbonate complexes of Be and eventually resulted in the precipitation of beryl in particular in the limestones and the contact zone between limestones and slates (e.g., Wood 1992).

In Stage II, the mineral assemblages of the hydrothermal veins in both limestone and slates are identical, which reflects that the minerals that had precipitated during Stage I shielded the fluids from interacting with the local wall-rocks. The absence of W and Be minerals in Stage II mineral assemblages may reflect that late fluids did not carry these elements at similar levels as Stage I fluids. Alternatively, the absence of scheelite, wolframite, and beryl may indicate that the lack of wall-rock interaction did not change the fluid composition and, thus, did not induce precipitation of these ore minerals.

### 5.2. *Wall-rock control on mineral chemistry of mica and scheelite*

The interaction between fluid and wall rocks during Stage I, in particular the dissolution of the carbonate wall rocks, did not only affect the mineral assemblage in the vein, but also the mineral chemistry. The

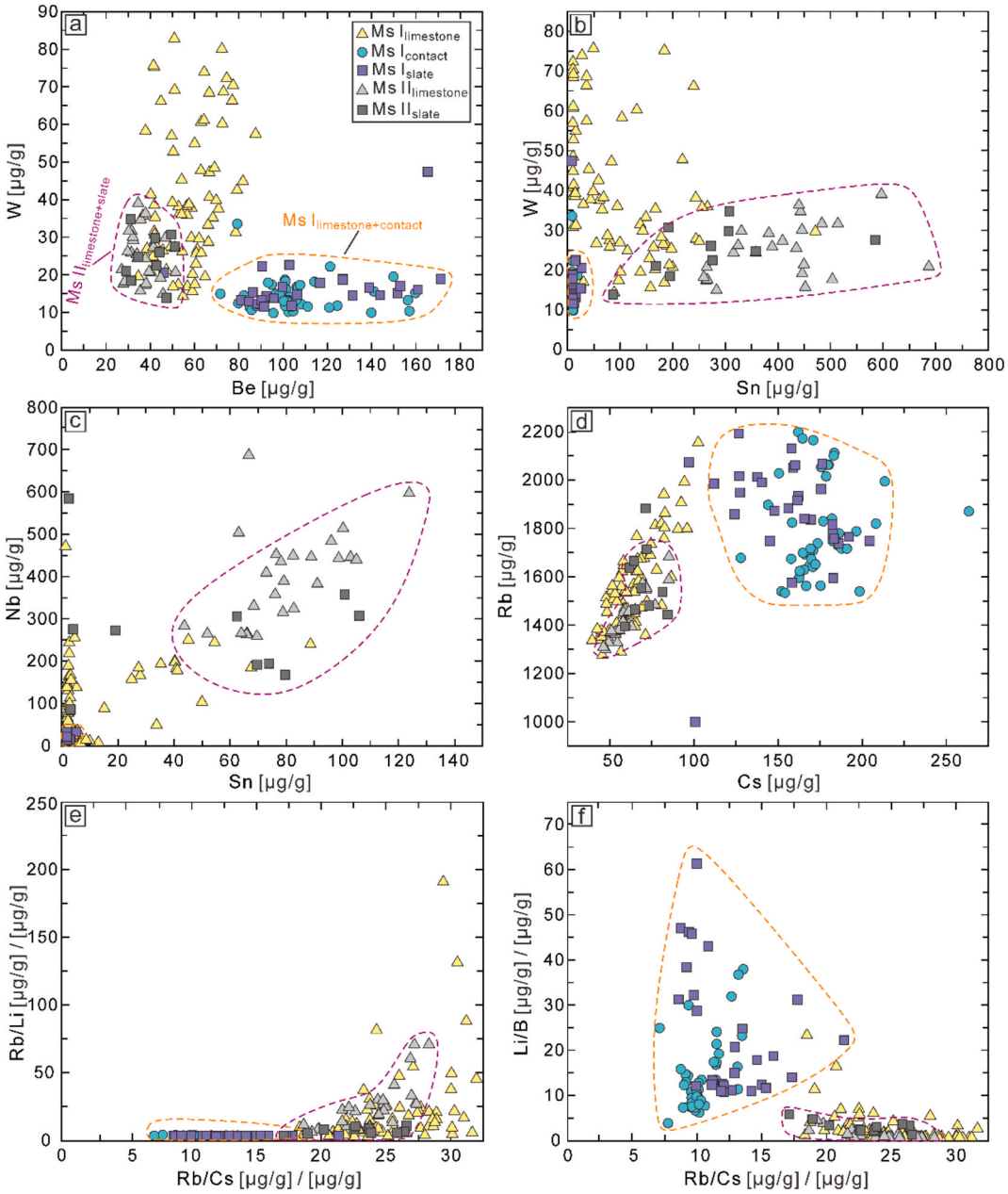


**Fig. 9.** Binary diagrams for mica from the Mahuaping deposit. (a) W vs. Be, (b) W vs. Sn, (c) Nb vs. Sn, (d) Rb vs. Cs, (e) Rb/Li vs. Rb/Cs, and (f) Li/B vs. Rb/Cs diagrams. Note the trace element contents and trace element ratios in Stage I mica depends on the immediate wall-rock that may act as source or stabilize phases that scavenge these trace elements. For discussion see text.

composition of mica in veins in the limestone is near the muscovite end-member, whereas the compositions of mica in the siliciclastic rocks is phengite (Fig. 5). Mica in the contact zone bridges the compositional gap between the two types, indicating that the nature of the surrounding rocks has a significant impact on the mica composition (e.g., Bishop and Bird, 1987). The contents of $SiO_2$, MgO, FeO, F, Be, Li, Rb, and Cs increase from the limestone wall-rocks, through the contact zone, to the siliciclastic rocks, whereas the contents of W, Nb, Ta, Sn, and Sr decrease. These compositional changes reflect contrasting availability of elements derived from the wall-rocks and the presence of phases that sequester elements that could be incorporated in mica. For instance, the dissolution of wall-rock limestone releases Ca, as well as Sr and possibly Pb that readily substitute for Ca. These elements do not enter the crystal lattice of muscovite to a significant extent. Instead, Ca reacts with F in the fluid to precipitate large amount of fluorite ($CaF_2$), eventually reducing the availability of F to be incorporated in mica and accounting for the relatively low F contents in Stage I mica in limestone-hosted veins. The precipitation of fluorite also triggers the precipitation of beryl. Therefore, Stage I muscovite in veins in limestone has lower Be contents than Stage I muscovite in veins in the slates (Fig. 9a). The dissolution of limestone in the Mahuaping deposit does not release significant amounts of Mg and, therefore, Stage $I_{limestone}$ mica does not have particularly high Mg-contents.

In contrast, the interaction of the fluids with the slates releases a wide range of elements. For instance, the dissolution of quartz and oxidation of pyrite releases Si and Fe, respectively, and the alteration of biotite to chlorite releases Fe, Mn, Mg, and F (which reach the highest contents in Stage $I_{slate}$ mica), but also K and elements substituting for K. The decrease of K/Rb ratios in mica from veins in limestones to the contact zone and the slates (Fig. 8) largely reflects the higher availability of Rb in slate-hosted veins. As the contents of K, which is controlled by mineral stoichiometry, do not vary significantly in muscovite and

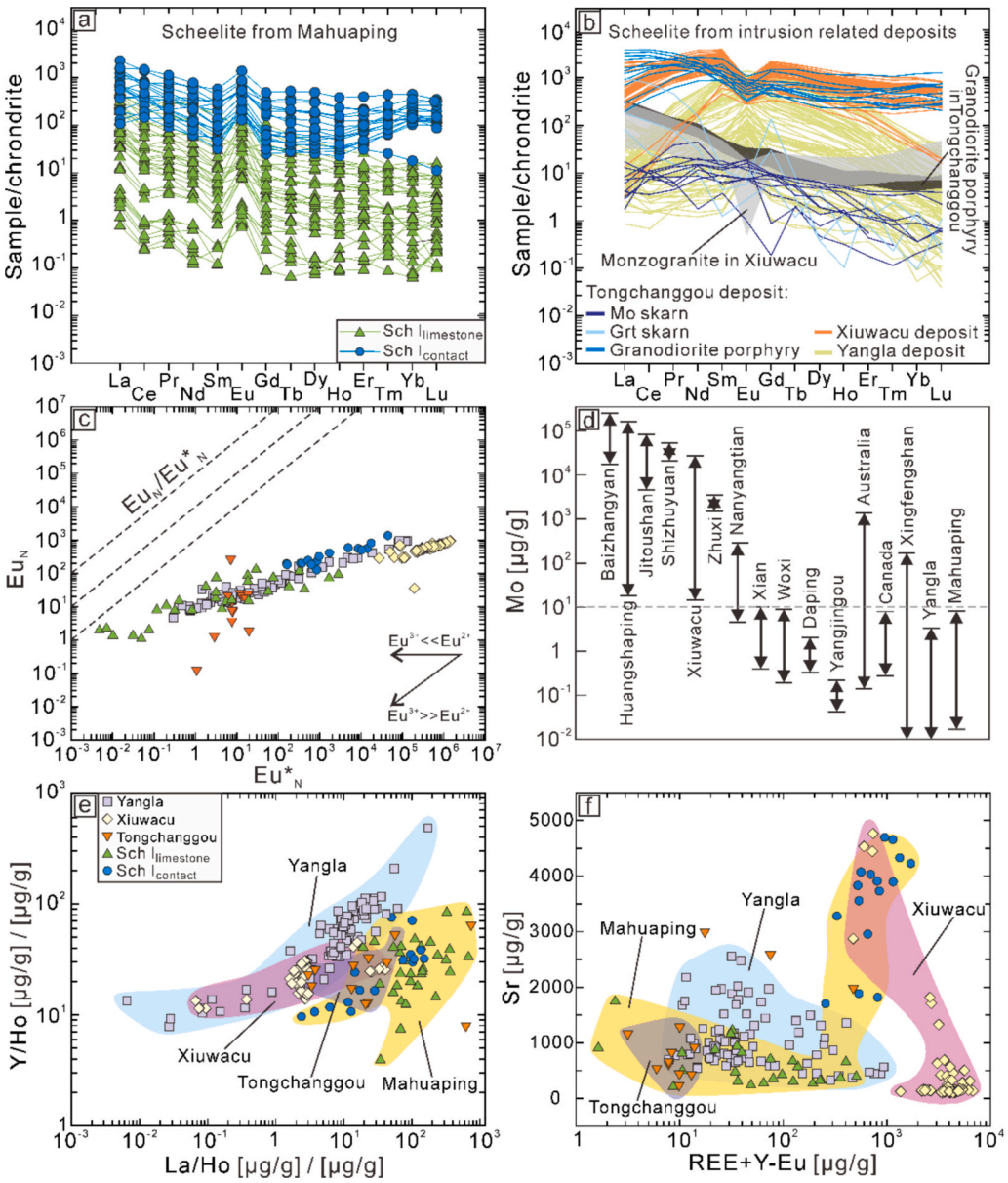


**Fig. 10.** Trace element and REE variation in scheelite. Chondrite-normalized distribution patterns of REE in scheelite from (a) Mahuaping and (b) the granite-related Xiuwacu, Tongchanggou, and Yangla deposits. Data from Zhang et al. (2017), Duan et al. (2024), and Li et al. (2023). Normalization values from McDonough and Sun (1995). (c) EuN/Eu* ratios for scheelite from the Mahuaping, Xiuwacu, Tongchanggou, and Yangla deposits. Data sources as for panels a and b. (d) Molybdenum content in scheelite from tungsten deposits. Data from Song et al. (2014), Ding et al. (2018), Wang et al. (2020a), Liu et al. (2017), Wang et al. (2020b), Zhang et al. (2021), Wen et al. (2022), Xiong et al. (2006), Ren et al. (2010), Ghaderi et al. (1999), Dostal et al. (2009), and Lei et al. (2023). (e) La/Ho–Y/Ho and f) REE + Y-Eu–Sr diagrams for scheelite from the Mahuaping, Xiuwacu, Tongchanggou, and Yangla deposits. Data sources as in panels a and b.

phengite, the variation of K/Rb is related to the availability of Rb for substitution into the interlayer site occupied by K. Higher contents of F, Si, Mg, Be, Li, and Sn at lower K/Rb (Fig. 8) indicate that these elements may have been added from the wall rocks to the fluid or that these elements were not scavenged from the fluid by other minerals.

Stage II mica, independent of the wall-rocks of the veins, defines an elongated cluster in the mica classification diagram (Fig. 5) that extends from the muscovite end-member composition toward the phengite field, but differs from the trend defined by Stage I mica. The compositional ranges of Stage $II_{limestone}$ and Stage $II_{slate}$ mica broadly overlap, indicating that the wall-rock has little or no influence on the composition of Stage II mica. Most major elements have similar compositional ranges as Stage I mica from limestone-hosted veins. Only the Fe contents seem to be distinctly higher in Stage II mica. The trace element contents of Stage II mica fall in two groups: (i) the contents of Li, Rb, Cs, Be, Sr and W are similar to those of Stage $I_{limestone}$ mica, but generally lower than those of Stage $I_{slate}$ mica (Fig. 9). Only Sr has higher contents than Stage $I_{slate}$ mica and W contents seem to be independent of the wall rock. (ii) Stage II mica has higher contents of Nb, Ta, and Sn than Stage I mica (independent of the wall rock). These higher contents may reflect that there are no mineral phases that scavenge these elements along the migration path of the fluid or that the contents of these elements in the fluid changed over the lifetime of the mineralizing system.

The important implication of the compositional data of the various mica types is the following: The composition of Stage I mica varies depending on the local wall-rocks. Once early crystallizing mineral assemblages prevent direct interaction between fluids and wall-rocks, the mica composition depends mainly on the fluid composition. Therefore, the composition of Stage II mica does not vary with the type of wall-rock.

Scheelite crystallized in hydrothermal fluids reacting with carbonate

host rocks captures the characteristics of both the fluids and the carbonate rocks (Li et al., 2021b; Ji et al., 2024). High trace elements contents in scheelite do not only reflect that these elements were transported by the fluid and, thus, were available for substitution, but also that these elements could be substituted into lattice sites occupied by Ca or W (Ghaderi et al., 1999; Brugger et al., 2000). In scheelite, Ca can be substituted by Sr and other divalent elements (e.g., Pb, Eu) and, to a certain extent, by trivalent ions (e.g., REEs), whereas W may be replaced by high field-strength ions Mo, Nb, and Ta (Ghaderi et al., 1999; Poulin et al., 2016). Thus, the low contents of Li, Be, B, Rb, Cs, and Ba reflect the incompatibility of these elements rather than their absence in the fluid (Poulin et al., 2016; Ji et al., 2024). On the other hand, elements that are highly compatible in scheelite may become depleted from the fluid during scheelite growth. Thus, the low contents of these elements (e.g., Mo, Nb, Ta) reflect the low abundance of these elements in the fluid (Ji et al., 2024), either as these elements have been removed from the fluid by earlier crystallizing scheelite or were never present in significant amounts in the fluid. In the Mahuaping deposit, the elements Mo, Nb, and Ta have low contents in scheelite. For instance, the Mo content is typically less than 1 μg/g and only rarely reaches up to 20 μg/g. For comparison, Mo in early-crystallized skarn scheelite may reach several thousand μg/g (e.g., Ji et al., 2024). We interpret the consistently low Mo contents in scheelite to reflect that Mo was not transported by the relatively oxidized fluid to a significant extent. Similarly, the consistently low Nb and Ta contents in scheelite (and mica) also may indicated that these elements were not particularly abundant in the fluids. The latter point is supported by the Nb and Ta contents of Stage I mica that are higher in veins in the slates than in the limestones.

### 5.3. Possible sources of fluids and ore elements

Primary W (−Sn) deposits typically form from late-stage magmatic fluids derived from highly evolved granites (Yuan et al., 2019; Cao et al., 2020; Monnier et al., 2022; Ni et al., 2024; Zhu et al., 2024). No granite bodies have been discovered at depth or in the larger surroundings of the deposit. Therefore, possibility of alternative metal sources has to be taken in consideration. Sedimentary rocks are a possible source and the mobilization of metals during prograde metamorphism is an alternative process. For instance, vein-type W deposits may form from metamorphic fluids that are released from sedimentary rocks during prograde low-grade metamorphism (e.g., Crocket et al., 1986; Cave et al., 2017). Similarly, the alteration of sheet silicates may release K, Li, F, and Be (Lecumberri-Sanchez et al., 2017; Yan et al., 2024). Prograde metamorphism slate could provide both the fluid and the ore elements necessary to form a vein-type deposit as Mahuaping.

The trace element signature of scheelite seems to depend on the setting in which the deposits formed (e.g., Poulin et al., 2018; Sciuba et al., 2020). Scheelite from magmatic-hydrothermal deposits typically contain low Sr contents, high Nb, Ta, and Mo contents (Poulin et al., 2018; Sciuba et al., 2020; Liu et al., 2022; Miranda et al., 2022; Gao, 2023), as well as high As and V contents (Sciuba et al., 2020). In contrast, scheelite from the Mahuaping deposit has high Sr contents ranging from 213 to 4694 μg/g, low Mo below 7.10 μg/g), Nb (1.04–21.28 μg/g), and Ta (0.02– 0.11 μg/g) contents and low As and V contents near or below the detection limit (Table S3). Whereas the high Sr contents reflect the carbonate wall-rocks of the veins, the low contents of Mo, Nb, and Ta, as well as low As and V contents, indicate that these elements did not reach high concentrations in the fluid. Thus, the trace element signature of scheelite do not favor a magmatic-hydrothermal fluid source. Furthermore, REE pattern of scheelite from the Mahuaping deposit show positive Eu anomalies and weak or no negative Ce anomalies (Fig. 10a), which contrasts with REE pattern for scheelite from magmatic and skarn-type tungsten deposits (Fig. 10b). The La/Ho ratio of scheelite mirrors the REE pattern, and shows low values for bell-shaped and other LREE-depleted pattern (cf. Fig. 10b and e) and high values for samples with LREE-enriched pattern as those for Sch $I_{limestone}$ and Sch $I_{contact}$ of the Mahuaping deposit (Fig. 10e). As the REE and Y content in carbonate wall-rocks are low, decarbonization does not affect the REE budget and the Y/Ho ratio of the fluid. The higher Sr and Y contents in Sch $I_{contact}$ do not only reflect the addition of Sr from dissolution of limestone and the addition of Y from the slates. Instead, the high Sr contents also may reflect the absence of phases that scavenge Sr and/or REE + Y. The large variation of REE + Y contents to very low values in some Sch $I_{limestone}$ possibly are due the presence of other phases–such as fluorite–that can incorporate REE (Fig. 10f).

Scheelite may incorporate large amounts of Mo. Therefore, the Mo content of scheelite reflects the availability of Mo for incorporation and seems to differ among different genetic types of W deposits (Song et al., 2014; Poulin et al., 2018). Scheelite from intrusion-related deposits, such as Huangshaping, Baizhangyan, and Shizhuyuan, have generally high Mo contents. In contrast, scheelite from vein-type deposits in metamorphic terranes, such as the Xi'an W deposit, Woxi Au-Sb-W deposit, Au-W deposits of Western Australia and Nova Scotia (Canada), typically have low Mo contents (Fig. 10d). Scheelite from Mahuaping has very low Mo contents (Table S3).

Muscovite and phengite from veins in the Mahuaping deposits has high contents of Li, Rb, and Cs, as well as high Rb/Sr ratios (13–1630) (Fig. 7a and 8; Table S2), as well as high contents of the ore elements Be, F, Sn, and W (Figs. 8 and 9; Table S2). Although such chemical fingerprints are typical for deposits related to granites and porphyries (Yin et al., 2019, 2022; Cui et al., 2024), these signatures are not restricted to intrusion-related deposits. Instead, these elements may also be activated during the process of low-temperature prograde metamorphism or the dehydration or recrystallization of muscovite. For instance, during the process of low-grade to medium-grade metamorphism, muscovite may be replaced or may recrystallize, releasing alkali metal elements (such as K, Rb and Cs) and other trace elements (Kunz et al., 2022; Stepanov et al., 2024). Similarly, the dissolution of oxyhydroxides in the sediments may release elements originally adsorbed on them. Furthermore, sub-greenschist facies metamorphism may mobilize W from detrital rutile or titanite in siliciclastic sediments (Cave et al., 2017). Low-temperature (sub-greenschist facies) prograde metamorphism of marine sediments may produce copious amounts of low-saline fluids that represent former pore waters and fluids released during the replacement of clay minerals by low-grade metamorphic minerals (e.g., Fyfe et al., 1978). Such fluids can serve as transport agents and provide F and Cl to complex metals released from altered and dissolved minerals. For instance, at temperatures above 200–250 °C, Be forms soluble fluoride and or fluorocarbonate complexes (Wood 1992) and W forms soluble $H_2WO_4$, $HWO_4^-$, and $WO_4^{2-}$ complexes (Wang et al., 2019). At these temperatures, Sn forms soluble Cl and F complexes (Schmidt et al., 2020) and may be redistributed Sn during prograde metamorphism (Romer et al., 2022). Thus, the formation of W and Be minerals and the high Sn contents in muscovite (0.66–687 μg/g) in the Mahuaping deposit do not require a magmatic metal source.

Fluid inclusions in fluorite of the Mahuaping deposit point to $CO_2$ and F-rich low-temperature and low-salinity fluids (homogenization temperature: 180–260 °C, salinity: 3–8 wt% NaCl; Ma et al., 2020 and own unpublished data), which differs from magmatic W deposits that have inclusions with higher homogenization temperatures and salinities (Rui et al., 2003; Song et al., 2010; Song et al., 2011; Li et al., 2022; Cui et al., 2023). Fluorine may derive from the alteration of micas in the fluid source and $CO_2$ originates from the decarbonation reaction of carbonate wall-rocks. Thus, high F and $CO_2$ contents in the fluids cannot be used as evidence for a magmatic fluid source.

Major and trace element contents in muscovite and scheelite from the Mahuaping deposit indicate that the deposit can be related to prograde metamorphism of pelitic rocks that serve as source of both the fluids and the ore elements. The ore-forming fluids may have migrated along the fault in the tectonic contact zone between limestone and slate. In the Mahuaping area, the carbonates above the fault deformed in a brittle manner and steeply-dipping tension fractures developed. The

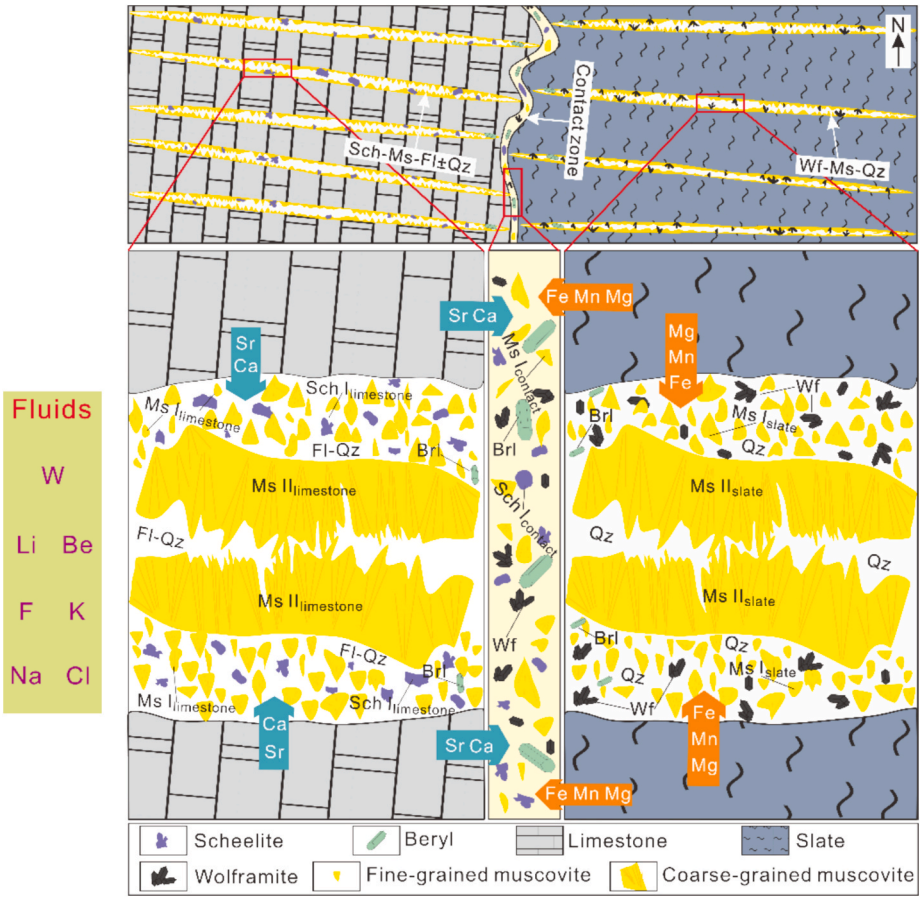


**Fig. 11.** Schematic diagram illustrating the source of material for the various vein stages and the different host rocks in the Mahuaping Be-W-F deposit. The contrasting mineral assemblages in early veins are directly related to the source of Ca (limestone) and Fe (slate). Abbreviations: Brl = beryl; Sch = scheelite; Wf = wolframite; Ms = muscovite; Fl = fluorite; Qz = quartz.

fluids escaped into these fractures and reacted with the wall rocks to precipitate mica, quartz, and ore minerals. The formation of mineralization in the limestone wall-rocks is controlled by carbonate dissolution. The released Ca induced precipitation of scheelite and fluorite, whereas the retraction of F from the fluid destabilized soluble Be complexes and resulted in the precipitation of beryl. In contrast, mineralization is related to the alteration of shale, which releases Fe and results in the precipitation of wolframite. Veins in the shale have only little fluorite and beryl (Fig. 11).

## 6. Conclusions

Fluids from low-grade metamorphic sedimentary rocks form Tertiary vein-type mineralization in the Mahuping Be-W-F deposit. Fluids migrated along the tectonic contact between Silurian limestones and Ordovician slates and mineralization formed at relatively shallow depths in steeply dipping tension fissures in these rocks near their flat contact zone. The mineral assemblages and the composition of mica in the fissures depends on the local wall rocks. The fissures were mineralized in two stages.

Low-temperature mineral assemblages of Stage I differ in veins in limestones and slates, with beryl, scheelite, fluorite, muscovite, and quartz in limestone and beryl, wolframite, muscovite, and quartz in slate. In the contact zone, scheelite and wolframite occur together with muscovite, quartz, fluorite, and beryl. The contrasting mineral assemblages are controlled by the nature of the wall-rocks. Dissolution of limestone releases Ca that induces to the precipitation of scheelite and fluorite. The removal of F from the fluid by fluorite precipitation destabilizes Be-complexes in the fluid and results in the precipitation of beryl. Alteration of slate provides Fe and results in the precipitation of wolframite rather than scheelite. Fluorite and beryl are less abundant in veins in the slates.

The composition of Stage I mica varies from muscovite in veins in the limestones to phengite in veins in the slates. The trace element content of mica depends on the fluid, the wall rocks of the veins and the presence of ore minerals that compete for the particular element. The wall-rock influence is illustrated by the higher Rb and Li contents in Stage I mica in veins in slates, whereas the presence of competing phases is illustrated by higher F and Be contents in Stage I mica in veins in slates as these veins have little or no fluorite and beryl, whereas veins in carbonates and the contact zone have variably abundant fluorite and beryl.

Stage I mica shields Stage II mica from interaction with the wall rocks. Therefore, the composition of Stage II mica does not vary with of the type of wall-rock.

## Declaration of competing interest

The authors declare that they have no known competing financial interests or personal relationships that could have appeared to influence the work reported in this paper.

## Acknowledgments

We are grateful to Zhonglin Ren and Bihong Zhang for their help during field work. We also appreciate the valuable comments and constructive reviews provided by the anonymous reviewers, which have significantly improved the quality of the paper. Additionally, we are

grateful to all the staff of the editorial department for their efforts in publishing this paper. This research was supported by the Selection Project of High-level Scientific and Technological Talents and Innovative Teams Project in Yunnan Province (202305AT350004 and 202205AS350015), the Major Scientific and Technological Projects in Yunnan Province (202202AG050006), and the National Natural Science Foundation of China (92055314).

## Appendix A. Supplementary data

Supplementary data to this article can be found online at https://doi.org/10.1016/j.oregeorev.2025.106728.

## Data availability

Data will be made available on request.

## References

Bishop, B.P., Bird, D.K., 1987. Variation in sericite compositions from fracture zones within the Coso Hot Springs geothermal system. Geochim. Cosmochim. Acta. 51, 1245–1256.
Brugger, J., Lahaye, Y., Costa, S., Lambert, D., Bateman, R., 2000. Inhomogeneous distribution of REE in scheelite and dynamics of Archaean hydrothermal systems (Mt. Charlotte and Drysdale gold deposits, Western Australia). Contrib. Mineral. Petrol. 139, 251–264.
Cao, H.W., Li, G.M., Zhang, Z., Zhang, L.K., Dong, S.L., Xia, X.B., Liang, W., Fu, J.G., Huang, Y., Xiang, A.P., Qing, C.S., Dai, Z.W., Pei, Q.M., Zhang, Y.H., 2020. Miocene Sn polymetallic mineralization in the Tethyan Himalaya, southeastern Tibet: a case study of the Cuonadong deposit. Ore Geol. Rev. 119, 103403.
Cave, B.J., Pitcairn, I.K., Craw, D., Large, R.R., Thompson, J.M., Johnson, S., 2017. A metamorphic mineral source for tungsten in the turbidite-hosted orogenic gold deposits of the Otago Schist, New Zealand. Miner. Deposita 52, 515–537.
Crocket, J.H., Fueten, F., Clifford, P.M., 1986. Distribution and localization of gold in Meguma group rocks, Nova Scotia: implications of metal distribution patterns in quartz veins and host rocks on mineralization processes at Harrigan Cove, Halifax County. Atl. Geol. 22, 15–33.
Cui, J.M., Ni, P., Peng, Z.Q., Pan, J.Y., Li, W.S., Ding, J.Y., Dai, B.Z., Gao, Y., Han, L., Zeng, Q., Zhang, T., 2023. Tungsten mineralization formed by single-pulsed magmatic fluid: evidence from wolframite-hosted fluid inclusion from the giant Dajishan "five floor" style W-polymetallic deposit. Ore Geol. Rev. 157, 105472.
Cui, J.Y., Meng, Y.K., Xiong, F.H., 2024. Petrogenesis of the miocene granitic porphyry in the middle gangdese belt: constraints from zircon U-Pb geochronology, whole-rock geochemistry and Sr-Nd-Hf-O isotopes. Acta Petrol. Sin. 40, 3734–3752 in Chinese with English abstract.
Dai, Z.W., Li, G.M., Xie, Y.L., Yang, Z.M., Huizenga, J.M., Liang, W., Fu, J.G., Cao, H.W., 2022. Source and evolution of the ore-forming fluid of the Cuonadong Sn-W-Be polymetallic deposit (southern Tibet, China): constraints from scheelite trace element and Sr isotope geochemistry. Ore Geol. Rev. 142, 0169–1368.
Ding, T., Ma, D.S., Lu, J.J., Zhang, R.Q., 2018. Garnet and scheelite as indicators of multi-stage tungsten mineralization in the Huangshaping deposit, southern Hunan province, China. Ore Geol. Rev. 94, 193–211.
Dostal, J., Kontak, D.J., Chatterjee, A.K., 2009. Trace element geochemistry of scheelite and rutile from metaturbidite-hosted quartz vein gold deposits, Meguma Terrane, Nova Scotia, Canada: genetic implications. Miner Petrol. 97, 95–109.
Duan, Z.Y., Zhang, Y.M., Yang, X.Q., Du, B., Wu, J.J., Yang, F.C., Jiang, X.J., 2024. Geochronology and whole-rock geochemistry of intrusive rocks from the Donglufang Cu-Mo deposit in western margin of the Yangtze block and their metallogenic implications. Acta Geosci. Sinica 45, 515–529 in Chinese with English abstract.
Fyfe, W.S., Price, N.J., Thompson, A.B., 1978. Fluids in the Earth's Crust. Elsevier, Amsterdam, p. 383.
Gao, F.F., 2023. Mica Geochemistry of the Xianghualing tin-Polymetallic Deposit in Southern Hunan and Its Indicative Significance for Mineralization. East China Univ. Sci. Tech., Jiangxi.
Ghaderi, M., Palin, J.M., Campbell, I.H., Sylvester, P.J., 1999. Rare earth element systematics in scheelite from hydrothermal gold deposits in the Kalgoorlie-Norseman region, Western Australia. Econ. Geol. 94, 423–437.
Gomes, M.E.P., Neiva, A.M.R., 2000. Chemical zoning of muscovite from the Ervedosa granite, northern Portugal. Mineral. Mag. 64, 347–358.
He, C.T., Qin, K.Z., Li, J.X., Zhou, Q.F., Zhao, J.X., Li, G.M., 2020. Preliminary study on occurrence status of beryllium and genetic mechanism in Cuonadong tungsten-tin-beryllium deposit, eastern Himalaya. Acta Petrol Sinica 36, 3593–3606 in Chinese with English abstract.
Heinrich, W., 2007. Fluid immiscibility in metamorphic rocks. Rev. Mineral. Geochem. 65, 389–430.
Hu, Z.H., Zhang, W., Liu, Y.H., Gao, S., Li, M., Zong, K.Q., Chen, H.H., Hu, S.H., 2015. "Wave" signal smoothing and mercury removing device for laser ablation quadrupole and multiple collector ICP-MS analysis: application to lead isotope analysis. Anal. Chem. 87, 1152–1157.
Ji, Y.H., Xie, G.Q., Romer, R.L., Li, W., Zhu, Q.Q., Fu, B., 2024. Scheelite composition fingerprints pulsed flow of magmatic fluid in the Fujiashan W skarn deposit, eastern China. Am. Mineral. 109, 747–763.
Jia, F.D., Zhang, C.Q., Hua, Z.X., Lou, D.B., Li, B.L., Sun, J., 2020. Identification characteristic, composition and genesis of euclase in Mahuaping tungsten-beryllium polymetallic deposit in Yunnan province. Spectrosc. Spectr. Anal. 40, 3185–3192 in Chinese with English abstract.
Kunz, B.E., Warren, C.J., Jenner, F.E., Harris, N.B.W., Argles, T.W., 2022. Critical metal enrichment in crustal melts: the role of metamorphic mica. Geology 50, 1219–1223.
Lecumberri-Sanchez, P., Vieira, R., Heinrich, C.A., Pinto, F., Wälle, M., 2017. Fluid-rock interaction is decisive for the formation of tungsten deposits. Geology 45, 579–582.
Lei, J.Z., Zhang, Y., Shi, C.H., Zhao, L.J., Cheng, Y.L., Shen, H.J., 2023. Geochemical characteristics of scheelite from Xingfengshan Au-W deposit in Xiangzhong metallogenic belt: implications on ore genesis. Mineral Deposits 42, 618–638 in Chinese with English abstract.
Li, B., Yang, X.B., Wang, X.F., Huang, Z.L., Tang, Y.W., Liu, Y.D., 2023. Genesis of tungsten mineralization in the Yangla copper-polymetallic deposit, northwest Yunnan, China: evidence from in situ U-Pb dating, trace elements, Sr isotopes, fluid inclusions, and H-O isotopes of scheelite. Gondw. Res. 129, 167–192.
Li, J., Huang, X.L., Fu, Q., Li, W.X., 2021a. Tungsten mineralization during the evolution of a magmatic-hydrothermal system: mineralogical evidence from the Xihuashan rare-metal granite in South China. Am. Mineral. 106, 443–460.
Li, P., Li, J.K., Chen, Z.Y., Liu, X., Huang, Z.B., Zhou, F.C., 2021b. Compositional evolution of the muscovite of Renli pegmatite-type rare-metal deposit, northeast Hunan, China: implications for its petrogenesis and mineralization potential. Ore Geol. Rev. 138, 104380.
Li, W.C., Wang, J.H., He, Z.H., Dou, S., 2016. Formation of Au-polymetallic ore deposits in alkaline porphyries at Beiya, Yunnan, Southwest China. Ore Geol. Rev. 73, 241–252.
Li, W.S., Ni, P., Pan, J.Y., Vivo, B.D., Albanese, S., Fan, M.S., Gao, Y., Zhang, D.X., Chi, Z., 2022. Co-genetic formation of scheelite- and wolframite-bearing quartz veins in the Chuankou W deposit, South China: evidence from individual fluid inclusion and wall-rock alteration analysis. Ore Geol. Rev. 142, 104723.
Lin, W.W., Peng, L.J., 1994. The estimation of $Fe^{3+}$ and $Fe^{2+}$ contents in amphibole and biotite from EPMA data. J. Changchun Univ. Earth Sci. 24, 155–162 in Chinese with English abstract.
Liu, C.X., Sun, F.Y., Li, J.Q., Han, J., Qian, Y., Zhang, Y.J., Hui, C., Bakht, S., 2022. The petrogenesis and metallogenesis of the Chakabeishan Li-Be pegmatitic deposit in Qinghai, NW China: evidence from geochronology, geochemistry, and mineral geochemistry. Ore Geol. Rev. 150, 105186.
Liu, S.B., Liu, Z.Q., Wang, C.H., Wang, D.H., Zhao, Z., Hu, Z.H., 2017. Geochemical characteristics of REEs and trace elements and Sm-Nd dating of scheelite from Zhuxi giant tungsten deposit in northeast Jiangxi. Earth Sci. Front. 24, 17–30 in Chinese with English abstract.
Liu, Y.S., Hu, Z.C., Gao, S., Günther, D., Xu, J., Gao, C.G., Chen, H.H., 2008. In situ analysis of major and trace elements of anhydrous minerals by LA-ICP-MS without applying an internal standard. Chem. Geol. 257, 34–43.
Ma, J., Tao, Y., He, D.F., Xiong, F., 2020. The ore-forming age and fluid inclusion characteristics of the Mahuaping tungsten-beryllium deposit in Yunnan Province. Bull. Mineral. Petrol. Geochem. 39, 223–232 in Chinese with English abstract.
McDonough, W.F., Sun, S.S., 1995. The composition of the Earth. Chem. Geol 120, 223–253.
Metcalfe, I., 2013. Gondwana dispersion and Asian accretion: tectonic and palaeogeographic evolution of eastern Tethys. J. Asian Earth Sci. 66, 1–33.
Miranda, A.C.R., Beaudoin, G., Rottier, B., 2022. Scheelite chemistry from skarn systems: implications for ore-forming processes and mineral exploration. Min. Deposita 57, 1469–1497.
Monnier, L., Salvi, S., Melleton, J., Lach, P., Pochon, A., Bailly, L., Béziat, D., Parseval, P. D., 2022. Mica trace-element signatures: highlighting superimposed W-Sn mineralizations and fluid sources. Chem. Geol. 600, 120866.
Ni, P., Chen, Y.J., Cheng, Y.B., Deng, X.H., 2024. Special issue of "China's W-Sn deposits". Ore Geol. Rev. 176, 106427.
Ni, P., Pan, J.Y., Han, L., Cui, J.M., Gao, Y., Fan, M.S., Li, W.S., Chi, Z., Zhang, K.H., Cheng, Z.L., Liu, Y.P., 2023. Tungsten and tin deposits in South China: temporal and spatial distribution, metallogenic models and prospecting directions. Ore Geol. Rev. 157, 105453.
Peng, H.W., Yang, L.L., Lai, J.Q., Li, B., Liu, X.H., Dai, Z.H., 2023. Mica geochemistry as an indicator of magmatic-hydrothermal processes in the Ta-Nb-Sn-W mineralization of the Limu deposit, South China. Ore Geol. Rev. 160, 0169–1368.
Pirajno, F., 2009. Hydrothermal processes and wall rock alteration. Hydrothermal Processes and Mineral Systems. Springer, Dordrecht.
Poulin, R.S., Kontak, D.J., McDonald, A., McClenaghan, M.B., 2018. Assessing scheelite as an ore-deposit discriminator using its trace-element and REE chemistry. Can. Mineral. 56, 265–302.
Poulin, R.S., McDonald, A.M., Kontak, D.J., McClenaghan, M.B., 2016. On the relationship between cathodoluminescence and the chemical composition of scheelite from geologically diverse ore-deposit environments. Can. Mineral. 54, 1147–1173.
Ran, M.J., Zhong, K.H., Li, F.Y., Luo, M.F., Liu, Z.C., Tang, J.X., 2011. Analysis of the tectonic of deposit and the age of mineralization in Mahuaping of Shangri-La in Yunnan. Sichuan Nonferrous Metals (02),, 21–27 in Chinese with English abstract.
Ren, Y.S., Zhao, H.L., Lei, E., Wang, H., Ju, N., Wu, C.Z., 2010. Trace element and rare earth element geochemistry of the scheelite and ore genesis of the Yangjingou large scheelite deposit in Yanbian area, northeastern China. Acta Petrol Sinica 26, 3720–3726 in Chinese with English abstract.

Romer, R.L., Kroner, U., Schmidt, C., Legler, C., 2022. Mobilization of tin during continental subduction-accretion processes. Geology 50, 1361–1365.
Rui, Z.Y., Li, M.Q., Wang, L.S., Wang, Y.T., 2003. Approach to ore-forming conditions in light of ore fluid inclusions. Min. Deposits 22, 13–23 in Chinese with English abstract.
Sciuba, M., Beaudoin, G., Grzela, D., Makvandi, S., 2020. Trace element composition of scheelite in orogenic gold deposits. Min. Deposita 55, 1149–1172.
Schmidt, C., Romer, R.L., Wohlgemuth-Ueberwasser, C.C., Appelt, O., 2020. Partitioning of Sn and W between granitic melt and aqueous fluid. Ore Geol. Rev. 117, 103263.
Song, G.X., Qin, K.Z., Li, G.M., 2010. Study on the fluid inclusions and S-H-O isotopic compositions of skarn–porphyry-type W–Mo deposits in Chizhou area in the middle–lower Yangtze Valley. Acta Petrol. Sinica 26, 2768–2782 in Chinese with English abstract.
Song, G.X., Qin, K.Z., Li, G.M., Evans, N.J., Chen, L., 2014. Scheelite elemental and isotopic signatures: implications for the genesis of skarn-type W-Mo deposits in the Chizhou area, Anhui Province, Eastern China. Am. Mineral. 99, 303–317.
Song, S.Q., Hu, R.Z., Bi, X.W., Wei, W.F., Shi, S.H., 2011. Hydrogen, oxygen and sulfur isotope geochemical characteristics of Taoxikeng tungsten deposit in Chongyi County, southern Jiangxi Province. Mineral Deposits 30, 1–10 in Chinese with English abstract.
Song, S.W., Mao, J.W., Romer, R.L., Jian, W., 2023. The petrogenesis of the Yangchuling porphyry W-Mo deposit, South China, an oxidized tungsten systems. Contrib. Mineral. Petrol. 178, 39.
Stepanov, A.S., Allen, C.M., Jiang, S.Y., Zhukova, I.A., Duan, D.F., Wang, L., 2024. Geochemistry of metasedimentary restitic rocks and implications for melting conditions and metal potential of crustal felsic magmas. Earth Sci. Rev. 254, 104799.
Sun, K.K., Deng, J., Wang, Q.F., Chen, B., Xu, R., Ma, Z.F., 2023. Formation of Sn-rich granitic magma: a case study of the highly evolved Kafang granite in the Gejiu tin polymetallic ore district, South China. Min Deposita 58, 359–378.
Tischendorf, G., Gottesmann, B., Förster, H.J., Trumbull, R.B., 1997. On Li-bearing micas: estimating Li from electron microprobe analyses and an improved diagram for graphical representation. Min. Mag. 61, 809–834.
Wang, X.S., Timofeev, A., Williams-Jones, A.E., Shang, L.B., Bi, X.W., 2019. An experimental study of the solubility and speciation of tungsten in NaCl-bearing aqueous solutions at 250, 300, and 350°C. Geochim. Cosmochim. Acta 265, 313–329.
Wang, Y., Tang, J.X., Wang, L.Q., Huizenga, J.M., Santosh, M., Zheng, S.L., Hu, Y., Gao, T., 2020a. Geology, geochronology and geochemistry of the Miocene Jiaoxi quartz-vein type W deposit in western Lhasa terrane, Tibet: implications for ore genesis. Ore Geol. Rev. 120, 103343.
Wang, Z.Q., Li, C., Jiang, X.J., Zhou, L.M., Zhao, J.J., Yan, Q.G., Chen, Y.K., 2020b. In situ trace element and Sr isotope composition of scheelite in the Xiuwacu molybdenum–tungsten deposit, Northwest Yunnan: constraints on mineralization. Rock Min. Anal. 39, 762–776 in Chinese with English abstract.
Wen, J., Hu, A.X., Peng, J.T., 2022. Geochemistry of scheelite in the Xi'an tungsten deposit western Hunan, and its implications for its ore genesis. Geol. Rev. 68, 1772–1788 in Chinese with English abstract.
Wood, S.A., 1992. Theoretical prediction of speciation and solubility of beryllium in hydrothermal solution to 300°C at saturated vapor pressure: application to bertrandite/phenakite deposits. Ore Geol. Rev. 7, 249–278.
Xiong, D.X., Sun, X.M., Shi, G.Y., Wang, S.W., Gao, J.F., Xue, T., 2006. Trace elements, rare earth elements (REE) and Nd-Sr isotopic compositions in scheelites and their implications for the mineralization in Daping gold mine in Yunnan province, China. Acta Petrol. Sinica 22, 733–741 in Chinese with English abstract.
Xiong, F., Tao, Y., Deng, X.Z., 2015. Analysis of fluid inclusion characteristics and deposit genesis of the Mahuaping W-Be deposit in Yunnan. Acta Mineral Sinica 35, 353–354 in Chinese with English abstract.
Xu, R., Romer, R.L., Kroner, U., Deng, J., 2022. Tectonic control on the spatial distribution of Sn mineralization in the Gejiu Sn district. China. Ore Geol. Rev. 148, 105004.
Yan, T.T., Zhang, X.F., Zhang, B.M., Song, C.G., Li, W.J., Chi, Q.H., 2024. Fluid-rock interactions recorded by bulk-rock and mica compositions in the Xiuwacu granite-related quartz-vein W–Mo deposit, western Yunnan Province, China. Ore Geol. Rev. 165, 105904.
Yang, F.C., Romer, R.L., Jiang, X.J., Li, W.C., 2025. Recurrent granite-related mineralization along former Tethys sutures in southwestern China. Ore Geol. Rev. 180, 106584.
Yang, G.S., Wen, H.J., Ren, T., Xu, S.H., Wang, C.Y., 2020. Geochronology, geochemistry and Hf isotopic composition of Late Cretaceous Laojunshan granites in the western Cathaysia block of South China and their metallogenic and tectonic implications. Ore Geol. Rev. 117, 103297.
Yang, S.Y., Jiang, S.Y., Mao, Q., Chen, Z.Y., Rao, C., Li, X.L., Li, W.C., Yang, W.Q., He, P. L., Li, X., 2022. Electron probe microanalysis in geosciences: analytical procedures and recent advances. At. Spectr. 43, 186–200.
Yin, R., Han, L., Huang, X.L., Li, J., Li, W.X., Chen, L.L., 2019. Textural and chemical variations of micas as indicators for tungsten mineralization: evidence from highly evolved granites in the Dahutang tungsten deposit, South China. Am. Mineral. 104, 949–965.
Yin, R., Huang, X.L., Wang, R.C., Sun, X.M., Tang, Y., Wang, Y., Xu, Y.G., 2022. Rare-metal enrichment and Nb–Ta fractionation during magmatic–hydrothermal processes in rare-metal granites: evidence from zoned micas from the Yashan Pluton, South China. J. Petro 63, 1–28.
Yuan, S.D., Williams-Jones, A.E., Romer, R.L., Zhao, P.L., Mao, J.W., 2019. Protolith-related thermal controls on the decoupling of Sn and W in Sn-W metallogenic provinces: insights from the Nanling Region, China. Econ. Geol. 114, 1005–1012.
Zhang, D.X., Pa, J.Y., Gao, J.F., Dai, T.G., Bayless, R.C., 2021. In situ LA ICP-MS analysis of trace elements in scheelite from the Xuefeng uplift belt South China and its metallogenic implications. Ore Geol. Rev. 133, 104097.
Zhang, X.F., Li, W.C., Yin, G.H., Yang, Z., Tang, Z., 2017. Geological and mineralized characteristics of the composite complex in Xiuwacu W-Mo mining district, NW Yunnan, China: constraints by geochronology, oxygen fugacity and geochemistry. Acta Petrol. Sinica 33, 2018–2036 in Chinese with English abstract.
Zhu, J., Tan, S.C., Yang, J.Y., He, X.H., Zhang, S.Q., Liu, Z., Wang, Y.C., 2024. What controls Sn-W mineralization in granite batholith: a case study from the world-class Dulong Sn-Zn polymetallic ore deposit of SW China. Ore Geol. Rev. 166, 105968.
Zong, K.Q., Klemd, R., Yuan, Y., He, Z.Y., Guo, J.L., Shi, X.L., Liu, Y.S., Hu, Z.C., Zhang, Z.M., 2017. The assembly of Rodinia: the correlation of early neoproterozoic (ca. 900Ma) high-grade metamorphism and continental arc formation in the southern Beishan Orogen, southern central Asian Orogenic Belt (CAOB). Precambr. Res. 290, 32–48.